Journal of the Korean Ceramic Society
Vol. 53, No. 4, pp. 400~405, 2016.

http://dx.doi.org/10.4191/kcers.2016.53.4.400

Photoactivities of Nanostructured α-Fe_2O_3 Anodes Prepared by Pulsed Electrodeposition

Mi Gyoung Lee and Ho Won Jang†

Department of Materials Science and Engineering, Research Institute of Advanced Materials, Seoul National University, Seoul 08826, Korea

(Received July 1, 2016; Revised July 18, 2016; Accepted July 18, 2016)

ABSTRACT

Ferric oxide (α-Fe_2O_3, hematite) is an n-type semiconductor; due to its narrow band gap (E_g = 2.1 eV), it is a highly attractive and desirable material for use in solar hydrogenation by water oxidation. However, the actual conversion efficiency achieved with Fe_2O_3 is considerably lower than the theoretical values because the considerably short diffusion length (2–4 nm) of holes in Fe_2O_3 induces excessive charge recombination and low absorption. This is a significant hurdle that must be overcome in order to obtain high solar-to-hydrogen conversion efficiency. In consideration of this, it is thought that elemental doping, which may make it possible to enhance the charge transfer at the interface, will have a marked effect in terms of improving the photoactivities of α-Fe_2O_3 photoanodes. Herein, we report on the synthesis by pulsed electrodeposition of α-Fe_2O_3-based anodes; we also report on the resulting photoelectrochemical (PEC) properties. We attempted Ti-doping to enhance the PEC properties of α-Fe_2O_3 anodes. It is revealed that the photocurrent density of a bare α-Fe_2O_3 anode can be dramatically changed by controlling the condition of the electrodeposition and the concentration of $TiCl_3$. Under optimum conditions, a modified α-Fe_2O_3 anode exhibits a maximum photocurrent density of 0.4 mA/cm^2 at 1.23 V vs. reversible hydrogen electrode (RHE) under 1.5 G simulated sunlight illumination; this photocurrent density value is about 3 times greater than that of unmodified α-Fe_2O_3 anodes.

Key words : α-Fe_2O_3, Pulsed electrodeposition, Water splitting, Doping, $TiCl_3$

1. Introduction

Solar driven water splitting with photoelectrochemical (PEC) reaction is a clean and effective way to produce hydrogen (H_2), a renewable and carbon-free fuel.[1-8] Because they suffer from inferior charge transport and broad band gap energies, photoanodes have low efficiency compared to that of photocathodes. Therefore, it is crucial to develop an efficient and practical anode system for the construction of high-performance PEC cells.[1-9]

Ferric oxide (α-Fe_2O_3, hematite) is a highly promising anode material for solar water oxidation because it can absorb a substantial portion of the visible spectrum due to its suitable band gap energy (~ 2.1 eV); it is also chemically stable in aqueous solution, abundant in the earth, and environmentally friendly.[10-14] However, α-Fe_2O_3 has limitations of low electron mobility (~10^{-2} cm^2/Vs) and short hole diffusion length (approximately 2-4 nm), as well as short life time of its carriers (~ 10 ps).[9-14] As a result, recombination losses lead to low photocurrent density and large overpotential for α-Fe_2O_3 based PEC water oxidation. For a reduction of the recombination losses of α-Fe_2O_3, great efforts have been devoted to nano-structuring and doping. The formation of nanostructures and the composition tuning (doping) of α-Fe_2O_3 are effective ways to overcome the limitations of this material's short hole-diffusion length and low electron mobility.[9-14]

The most commonly used methods to synthesize α-Fe_2O_3 photoanodes include spray pyrolysis, chemical vapor deposition, the sol-gel method, and anodization of iron metal.[9-14] Electrodeposition has also been demonstrated as a viable method to prepare α-Fe_2O_3 as nanostructured film photoelectrodes. With deposition potential and current as additional synthesis parameters, this solution-based method can be particularly beneficial for tuning the compositions and morphologies of deposits; this tuning process is reported to be crucial for improving the intrinsically poor charge transport properties of α-Fe_2O_3.[10-11,13-16] To synthesize α-Fe_2O_3 by electrodeposition, the use of a pulsed rather than a continuous voltage has several advantages.[17-19] Pulsed electrodeposition enables the formation of more uniform films than is possible using continuous electrodeposition because the pulse-off time (t_{off}) allows the diffusion of ions from the solution to the surface of the working electrode, thus lowering the concentration gradient during the next pulse-on time (t_{on}). Furthermore, pulsed electrodeposition can make more refined structure than is possible when using continuous deposition. We can confirm the different levels of uniformity achieved using pulsed electrodeposition and continuous deposition by the photographs of individual films. In addition, various thin film nanostructures can be formed by con-

†Corresponding author : Ho Won Jang
E-mail : hwjang@snu.ac.kr
Tel : +82-2-880-1720 Fax : +82-2-884-1413

trolling the sign and the amplitude of the pulsed voltages in pulsed electrodeposition.[17-19]

In this study, using pulsed electrodeposition, we fabricated nanostructured α-Fe_2O_3 thin films with elemental doping. The thickness and the morphology of the α-Fe_2O_3 thin films can be tailored simply by controlling the electrodeposition conditions such as the potential, time, and annealing condition. Also, the photoactivities of α-Fe_2O_3 anodes were found to differ significantly depending on the electrodeposition conditions. Although the linear sweep voltammetry (LSV) curves of our α-Fe_2O_3 films are comparable to those of previously reported α-Fe_2O_3 films, the photocurrent density of α-Fe_2O_3 films was significantly low at 1.23 V vs. RHE; thus, further improvements are needed to generate higher photocurrents. Therefore, to improve the photocurrent density of our α-Fe_2O_3 films, we introduced the doping of Ti and V. The optimum composition of α-Fe_2O_3 with Ti recorded a photocurrent density of 0.4 mA/cm^2 at 1.23 V vs. RHE, without additional catalyst. Therefore, the control of the morphology of nanostructured α-Fe_2O_3, and elemental doping, are shown to be the keys to achieving high PEC efficiency.

2. Experimental Procedure

2.1. Synthesis of nanostructured α-Fe_2O_3 anodes

Nanostructured α-Fe_2O_3 anodes were modified by pulsed anodic electrodeposition. In this study, an F: SnO_2 (FTO) substrate with dimensions of 1.5 × 1.5 cm and an active site region of 1.5 × 1.0 cm was defined with a shadow mask. Precursor was prepared by dissolving 0.02 M $FeCl_2 \cdot 5H_2O$ (99 %, Aldrich) at pH 4.1.[10] Before the deposition, FTO was cleaned with acetone, ethanol, and deionized water for 30 min, sequentially. Pulsed electrodeposition was conducted in a standard three electrode system with a working electrode of FTO, an Ag/AgCl reference electrode, and a platinum counter electrode. The entire procedure was carried out potentiostatically at 1.23 V vs. Ag/AgCl at 80°C (ca. 600 - 700 μA/cm^2) for 8, 12, 16, and 20 min. Then, all freshly prepared amorphous FeOOH samples were rinsed and annealed at 600°C for 2 h in air and then heated at 800°C for 1 min in a process of rapid thermal annealing (RTA). After annealing, the as-deposited films were converted to crystalline α-Fe_2O_3. We confirmed that increasing the deposition potential or the temperature promoted oxygen evolution and reduced the uniformity of the films. However, decreasing of the deposition potential or of the temperature reduced the deposition rate and led to the need for a longer deposition time to obtain a certain thickness.[10]

2.2. Doping of Ti and V on nanostructured α-Fe_2O_3 anodes

Desired amounts (0.1%, 1%) of titanium trichloride aqueous solution (20%, $TiCl_3$, Aldrich) were added to the electrodeposition solution to improve the PEC property of the nanostructured α-Fe_2O_3 films. Ammonium vanadate (99%, NH_4VO_3, Aldrich) was used for the doping of V.

2.3. Characterization

The morphologies of the nanostructured α-Fe_2O_3 films were characterized by field emission scanning electron microscopy (MERLIN Compact, JEOL). X-ray diffraction (XRD) characterization was performed to confirm the crystalline phase of the nanostructured α-Fe_2O_3 films.

2.4. PEC measurements

PEC measurements (Ivium Technologies, Nstat) were performed with a three electrode system using a 3 M Ag/AgCl reference electrode and a Pt mesh as the counter electrode in 1 M sodium hydroxide (NaOH, Wako) at pH 13. The photocurrent vs. potential curve was recorded while sweeping the potential range from –0.6 V to 0.8 V vs. Ag/AgCl in the positive direction with a scan rate of 25 mV/s under a solar simulator with an AM 1.5 G filter; the light intensity of the solar simulator was calibrated to 1 sun (100 mW/cm^2) using a reference cell. The measurement potential vs. Ag/AgCl was converted to the reversible hydrogen electrode scale according to the Nernst equation.

$$E_{RHE} = E_{Ag/AgCl} + 0.059\ pH + E^0_{Ag/AgCl}\ (E^0_{Ag/AgCl} = 0.1976)$$

3. Results and Discussion

A schematic of pulsed electrodeposition is presented in Fig. 1(a). The duration and amplitude of the voltage pulse used in this study to synthesize α-Fe_2O_3 films are shown in Fig. 1(c). The electrodeposition used in this study involves two reactions: the first is the oxidation of Fe^{2+} ions to Fe^{3+} ions; the second is the precipitation of Fe^{3+} ions as ferric oxyhydroxide (FeOOH) due to the limited solubility of Fe^{3+} ions in acidic aqueous solution (pH = 4.1).[10] The electrodeposited films were amorphous FeOOH and showed uniform, transparent, and yellow color. These films can be converted to crystalline α-Fe_2O_3 films by proper annealing, leading to an orange color. After annealing at 600°C for 2 h and then at

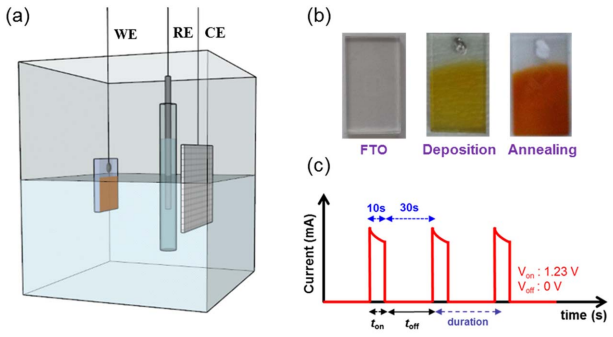

Fig. 1. (a) Schematic illustration of pulsed electrodeposition of α-Fe_2O_3 photoanodes for solar water splitting. (b) Photographic images of films after deposition and after annealing. (c) Pulsed electrodeposition of α-Fe_2O_3 films.

800°C for 1 min, all films exhibited uniform color and consisted of crystalline phase of α-Fe_2O_3.

The X-ray diffraction (XRD) patterns of the electrodeposited amorphous FeOOH and α-Fe_2O_3 films are presented in Fig. 2. The films showed representative peaks of α-Fe_2O_3, with preferred orientation in the (110) direction. The preferential growth along the (110) direction indicates that the most conductive plane (001) of the α-Fe_2O_3 films is aligned vertically to the substrate; this plane is reported to have higher photoactivity than those of the other planes.[10-11] The XRD data showed that the only difference between amorphous FeOOH and α-Fe_2O_3 films is that a specific peak near 45° emerges in the annealed films. Top and cross-sectional scanning electron microscopy (SEM) images of the nanostructured α-Fe_2O_3 films are shown in Fig. 3. The top-view SEM image shows the presence of cracks on the surface of the annealed films; this indicates that these films were thermally generated during annealing of cooling. The formation of densely packed α-Fe_2O_3 nanostructured films with average particle size of 30 nm and with open porosity is also evident. The cross-sectional SEM images show a film with an estimated thickness of ~ 150 nm, in which the particles are stacked, and good interfaces are formed between the Fe_2O_3 films and the FTO substrate.

PEC measurements of the α-Fe_2O_3 anodes were performed using a standard three-electrode cell with an electrolyte of 1 M sodium hydroxide at a scan rate of 10 mV/s under 1.5 G solar light. The photoelectrochemical current densities of the α-Fe_2O_3 anodes were plotted as a function of potential vs. RHE. The results of the LSV measurements are presented in Fig. 4(a). The films annealed at 600°C showed a negligible photocurrent density at 1.23 V vs. RHE; there was no difference between the light condition and dark condition. This means that high temperature annealing is required to activate the α-Fe_2O_3 anodes. The photoactivity of these films emerges after additional heat treatment at 800°C, which resulted in a water oxidation photocurrent density of about 0.1 mA/cm^2 at 1.23 V, as can be seen in Fig. 4(b). Through these results, we understand that

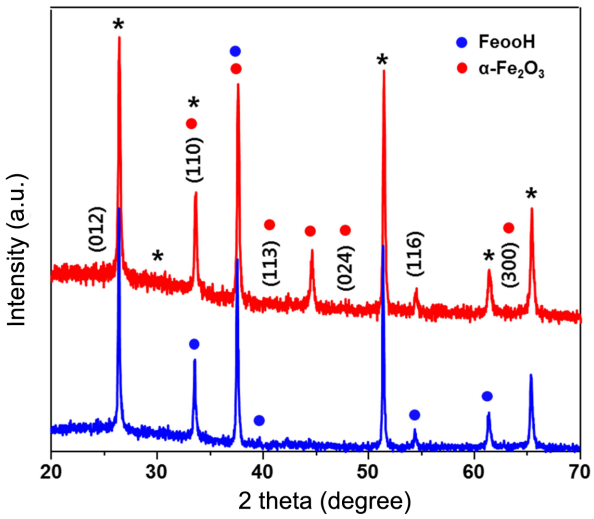

Fig. 2. X-ray diffraction (XRD) data of as-deposited and annealed films. Peaks from the FTO substrate are indicated by *.

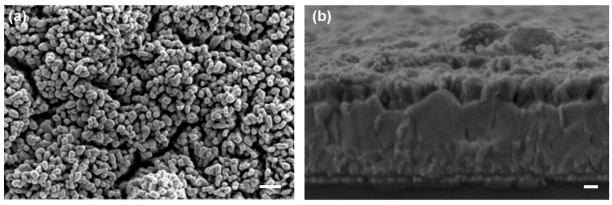

Fig. 3. Top and cross-sectional SEM images of the α-Fe_2O_3 films. Scale bar is 100 nm.

the effect of annealing temperature on the photoactivity of these photoanodes is significant. The effect of annealing at high temperature on the photoactivity of α-Fe_2O_3 anodes can be explained in two ways.[11,13-14] First, the unintentional diffusion of Sn from the FTO substrate to the film at high temperature annealing can contribute to an increase in the photocurrent by increasing the electronic conductivity of α-Fe_2O_3. Defects at the α-Fe_2O_3/FTO interface can be reduced by annealing at the high temperature. In addition, the pres-

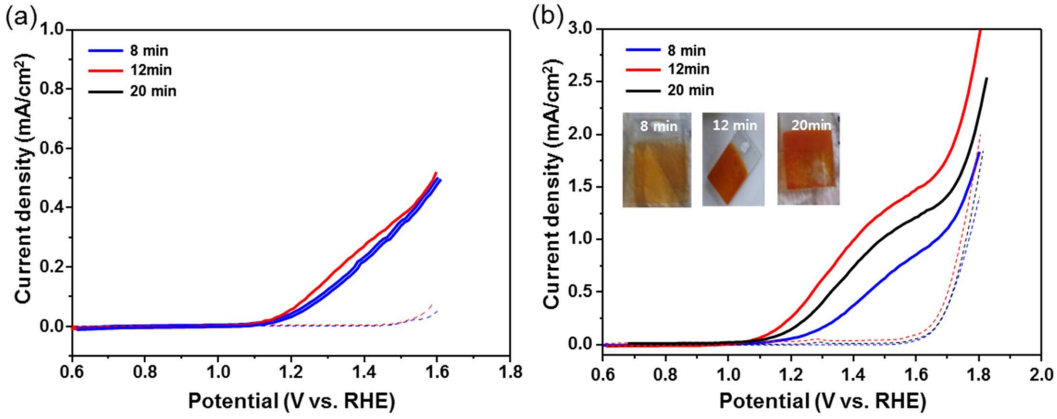

Fig. 4. Linear sweep voltammogram (LSVs) measurements of the α-Fe_2O_3 films by controlling deposition time. (a) Before, and (b) after annealing at the high temperature of 800°C.

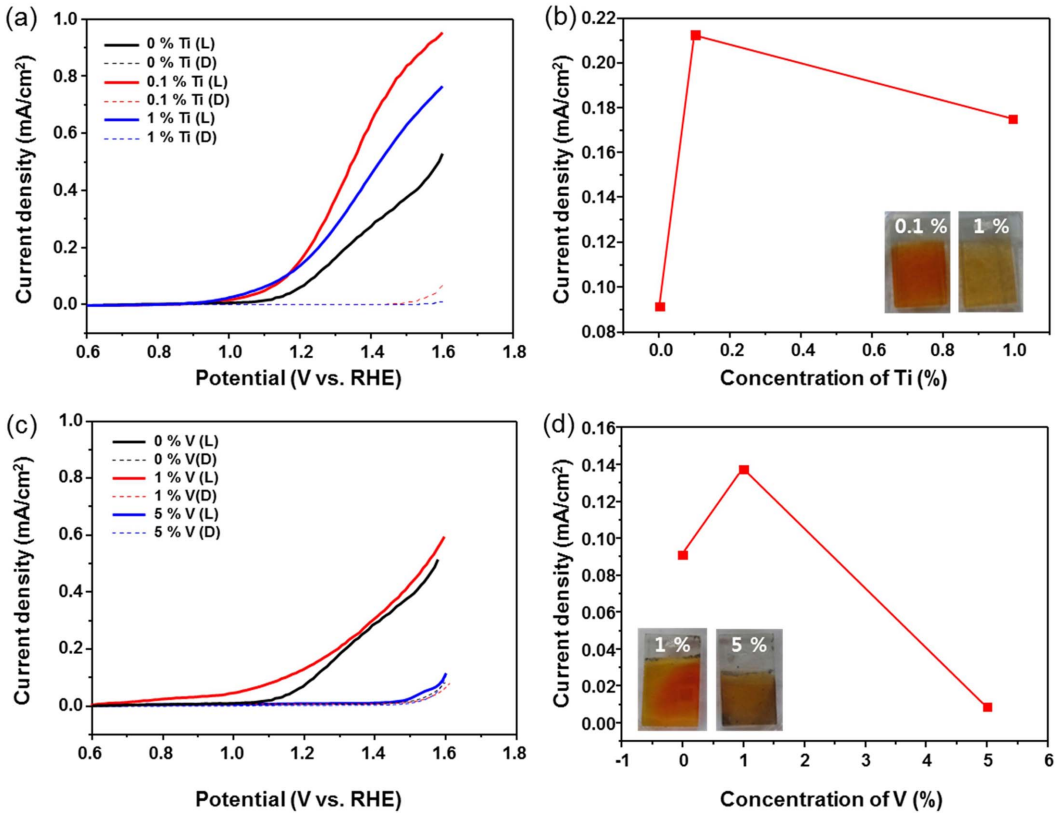

Fig. 5. (a), (c) LSV curves of the α-Fe_2O_3 films formed by changing the concentration of dopant, such as Ti and V. (b), (d) Amperometric current density-time profiles for Ti-doped and V-doped α-Fe_2O_3 films, respectively, at 1.23 V vs. RHE.

ence of cracks on the surface might enhance the photoactivity because these cracks allow electrolytes to reach the FTO surface and to increase the areas of the α-Fe_2O_3 films/electrolyte interface. Moreover, grain boundaries, which are likely the main limitation of electron and hole recombination, were removed after the high temperature annealing, thus improving the PEC performance of the α-Fe_2O_3 anodes.[11,13-14)]

The PEC performance of the α-Fe_2O_3 films was measured by altering the deposition time to change the thickness of the films, as shown in Fig. 4. Electrodeposition was performed for 8 - 12 min at 1.23 V vs. Ag/AgCl. The photocurrent density increased gradually until the deposition time increased to 12 min; the photocurrent density then started to decrease. A high photocurrent of 0.1 mA/cm^2 was obtained with of 12 min, which indicates that the photoactivity of α-Fe_2O_3 strongly depends on the film thickness. The initial increase in the photocurrent can be related to the increased amount of photoactive iron oxide on the FTO substrate, which in turn improves the light absorption efficiency.[10-14)] The absorbed photons can enlarge the number of photo-excited carriers and thus enhance the photocurrent density. In contrast, because it is hard to generate photo-excited carriers, a gradual decrease in the photocurrent density of the α-Fe_2O_3 films occurred for longer deposition times after the optimal deposition time was reached. Due to the greater penetration depths of low-energy photons, and the shorter hole diffusion length in α-Fe_2O_3, generated holes are less likely to reach the α-Fe_2O_3/electrolyte interface, and thus charge carrier recombination occurs.[10-14)] Based on these results, α-Fe_2O_3 films obtained with a 12 min deposition time and a thickness of about 150 nm appear to be ideal for efficient light absorption and reduced recombination loss. The linear sweep voltammetry (LSV) curves of our α-Fe_2O_3 films are comparable to those of previously reported α-Fe_2O_3 films (thickness ~ 150 nm); however, the photocurrent density of the α-Fe_2O_3 films was less than 0.5 mA/cm^2 at 1.23 V vs. RHE; thus, further improvements are needed to generate higher photocurrents.

To improve the PEC properties of α-Fe_2O_3 photoanodes, we employed elemental doping with Ti and V because most dopants such as Ti, Sn, and Si lead to an improvement of the PEC performance of α-Fe_2O_3 photoanodes, and because Ti^{4+} doping has been shown to greatly increase the photocurrent and to lead to better onset potential of the photoresponse.[20-23)] Doping has important roles in improving the donor density and the electrical conductivity. However, the PEC properties can be strongly influenced by the dopant concentration.[20-23)] Fig. 5(a) displays the LSV curves of Ti-doped α-Fe_2O_3 photoanodes. The photocurrent density increased after doping of 0.1% Ti; the onset potential of PEC water oxidation on Ti-doped α-Fe_2O_3 was improved by up to 100 mV. The photoactivity of Ti-doped α-Fe_2O_3 increases gradually until the doping concen-

tration reaches 0.1%; the photocurrent then starts to decrease, as is shown in Fig. 5(b). A photocurrent density of 0.22 mA/cm^2 was obtained at 1.23 V vs. RHE for the 0.1% Ti-doped α-Fe_2O_3 sample. Also, we observed the effect of V-doped α-Fe_2O_3, with results shown in Fig. 5(c). However, the V-doped α-Fe_2O_3 films show slightly lower photocurrents compared with those of the Ti-doped α-Fe_2O_3 films. The photocurrent of V-doped α-Fe_2O_3 has a slightly increased value of 0.13 mA/cm^2. And, it shows a tendency similar to that of Ti-doped α-Fe_2O_3: the photocurrent density starts to decrease when the concentration of dopant reach its optimum value, as shown in Fig. 5(d). Even though we tried to improve the PEC properties of the α-Fe_2O_3 films, the photoactivities of α-Fe_2O_3 are significantly lower than the theoretical efficiency (~ 10.5 mA/cm^2). Therefore, our α-Fe_2O_3 films have to be modified through the addition of co-catalysts, nanostructuring, and the formation of heterojunctions.

4. Conclusions

We synthesized α-Fe_2O_3 nanostructures using pulsed electrodeposition followed by high temperature annealing to activate α-Fe_2O_3. We studied the effect of the deposition time and the annealing conditions by changing these parameters for application to photoanodes in PEC cells. The results indicate that annealing at high temperature is necessary to activate α-Fe_2O_3 photoanodes and to increase the photocurrent. Also, optimal deposition time is essential to improve the PEC characteristics because the film thickness depends strongly on the deposition time. We further demonstrated an improvement of the PEC properties of α-Fe_2O_3 films by introducing doping with V and Ti. Ti-doped α-Fe_2O_3 films exhibit enhanced photocurrents (~ about 2.5 fold enhancement) compared to those of bare α-Fe_2O_3 films.

Acknowlegements

Mi Gyoung Lee acknowledges the Global Ph. D Fellowship Program through the National Research Foundation of Korea funded by the Ministry of Education. (2015H1A2A 1034356).

REFERENCES

1. X. Li, J. Yu, J. Low, Y. Fang, J. Xiao, and X. Chen, "Engineering Heterogeneous Semiconductors for Solar Water Splitting," *J. Mater. Chem. A*, **3** [6] 2485-534 (2015).
2. J. Goldemberg, "Ethanol for a Sustainable Energy Future," *Science*, **315** [5813] 808-10 (2007).
3. M. Gratzel, "Photoelectrochemical Cells," *Nature*, **15** [414] 338-44 (2001).
4. Z. Chen, H. N. Din, and E. Miller, Photoelectrochemical Solar Water Splitting; Vol. 1, pp.1-113, Springer, New York, 2013.
5. M. G. Walter, E. L. Warren, J. R. McKone, S. W. Boettcher, Q. Mi, E. A. Santori, and N. S. Lewis, "Solar Water Splitting Cells," *Chem. Rev.*, **110** [11] 6446-73 (2010).
6. M. S. Prevot and K. Sivula, "Photoelectrochemical Tandem Cells for Solar Water Splitting," *J. Phys. Chem. C,* **117** [35] 17879-93 (2013).
7. D. M. Andoshe, S. Choi, Y.-S. Shim, S. H. Lee, Y. Kim, C. W. Moon, D. H. Kim, S. Y. Lee, T. Kim, H. K. Park, M. G. Lee, J.-M. Jeon, K. T. Nam, M. Kim, J. K. Kim, J. Oh, and H. W. Jang, "A Wafer-Scale Antireflective Protection Layer of Solution-Processed TiO_2 Nanorods for High Performance Silicon-based Water Splitting Photocathodes," *J. Mater. Chem. A*, **4** [24] 9477-85 (2016).
8. K. C. Kwon, S. Choi, K. Hong, C. W. Moon, Y.-S. Shim, D. H. Kim, T. Kim, W. Sohn, J.-M. Jeon, C. H. Lee, K. T. Nam, S. Han, S. Y. Kim, and H. W. Jang, "Wafer-Scale Transferable Molybdenum Disulphide Thin-Film Catalyst for Photoelectrochemical Hydrogen Production," **9** [7] 2240-48 (2016).
9. D. M. Andoshe, J.-M. Jeon, S. Y. Kim, and H. W. Jang, "Two-Dimensional Transition Metal Dichalcogenide Nanomaterials for Solar Water Splitting," *Electron. Mater. Lett.*, **11** [3] 323-35 (2015).
10. R. L. Spray and K.-S. Choi, "Photoactivity of Transparent Nanocrystalline Fe_2O_3 Electrodes Prepared via Anodic Electrodeposition," *Chem. Mater.*, **21** [15] 3701-9 (2009).
11. G. Ranman and O.-S. Joo, "Photoelectrochemical Water Splitting at Nanostructured α-Fe_2O_3 Electrodes," *Int. J. Hydrogen Energy*, **37** [19] 13989-97 (2012).
12. L. Wang, C.-Y. Lee, and P. Schmuki, "Solar Water Splitting: Preserving the Beneficial Small Feature Size in Porous α-Fe_2O_3 Photoelectrodes during Annealing," *J. Mater. Chem. A*, **1** [2] 212-15 (2013).
13. L. Wang, C.-Y. Lee, and P. Schmuki, "Influence of Annealing Temperature on Photoelectrochemical Water Splitting of α-Fe_2O_3 Films Prepared by Anodic Deposition," *Electrochim. Acta*, **91** [28] 307-13 (2013).
14. K. Sivula, F. L. Formal, and M. Gratzel, "Solar Water Splitting: Progress Using Hematite (α-Fe_2O_3) Photoelectrodes," *ChemSusChem*, **4** [4] 432-49 (2011).
15. A. J. Bard and L. R. Faulkne, Electrochemical Methods; Vol. 2, pp.226-304, John Wiley & SONS, New York, 2001.
16. D. Kang, T. W. Kim, S. R. Kubota, A. C. Cardiel, H. G. Cha, and K.-S. Choi, "Electrochemical Synthesis of Photoelectrodes and Catalysts for Use in Solar Water Splitting," *Chem. Rev.*, **115** [23] 12839-87 (2015).
17. M. S. Chandrasekar and M. Pushpavanam, "Pulse and Pulse Reverse Plating—Conceptual, Advantages and Applications," *Electrochim. Acta*, **53** [8] 3313-22 (2008).
18. N. S. Qua, D. Zhua, and K. C. Chan, "Pulse Electrodeposition of Nanocrystalline Nickel Using Ultra Narrow Pulse Width and High Peak Current Density," *Surf. Coat. Technol.*, **168** [2-3] 123-28 (2003).
19. D. Gopi, J. Indira, and L. Kavitha, "A Comparative Study on the Direct and Pulsed Current Electrodeposition of Hydroxyapatite Coatings on Surgical Grade Stainless Steel," *Surf. Coat. Technol.*, **206** [11-12] 2859-69 (2012).
20. S. Shen, "Physical and Photoelectrochemical Characterization of Ti-doped Hematite Photoanodes Prepared by Solution Growth," *J. Mater. Chem. A*, **1** [46] 14498-506 (2013).
21. S. Li, P. Zhang, X. Song, and L. Gao, "Ultrathin Ti-doped Hematite Photoanode by Pyrolysis of Ferrocene," *Int. J.*

Hydrogen Energy, **39** [27] 14596-603 (2014).

22. R. Franking, L. Li, M. A. Lukowski, F. Meng, Y. Tan, R. J. Hamers, and S. Jin, "Facile Post-Growth Doping of Nanostructured Hematite Photoanodes for Enhanced Photoelectrochemical Water Oxidation," *Energy Environ. Sci.*, **6** [2] 500-12 (2013).
23. T. Y. Yang, H. Y. Kang, U. Sim, Y. J. Lee, J. H. Lee, B. Koo, K. T. Nam, and Y. C. Joo, "A New Hematite Photoanode Doping Strategy for Solar Water Splitting: Oxygen Vacancy Generation," *Phys. Chem. Chem. Phys.*, **15** [6] 2117-24 (2013).